Published in final edited form as:
Methods Enzymol. 2009 ; 457: 373–393. doi:10.1016/S0076-6879(09)05021-6.

Assessment of *In Vivo* Mitochondrial Metabolism by Magnetic Resonance Spectroscopy

Douglas E. Befroy[*], **Kitt Falk Petersen**[†], **Douglas L. Rothman**[‡], and **Gerald I. Shulman**[§]

[*]Departments of Diagnostic Radiology and Internal Medicine, Yale University School of Medicine, New Haven, Connecticut, USA

[†]Department of Internal Medicine, Yale University School of Medicine, New Haven, Connecticut, USA

[‡]Departments of Diagnostic Radiology and Biomedical Engineering, Yale University School of Medicine, New Haven, Connecticut, USA

[§]Departments of Internal Medicine and Cellular and Molecular Physiology, Howard Hughes Medical Institute, Yale University School of Medicine, New Haven, Connecticut, USA

Abstract

Magnetic resonance spectroscopy (MRS), a companion technique to the more familiar MRI scan, has emerged as a powerful technique for studying metabolism noninvasively in a variety of tissues. In this article, we review two techniques that we have developed which take advantage of the unique characteristics of ^{31}P and ^{13}C MRS to investigate two distinct parameters of muscle mitochondrial metabolism; ATP production can be estimated by using the ^{31}P saturation-transfer technique, and oxidation via the TCA cycle can be modeled from ^{13}C MRS data obtained during the metabolism of a ^{13}C-labeled substrate. We will also examine applications of the techniques to investigate how these parameters of muscle mitochondrial metabolism are modulated in insulin resistant and endurance trained individuals.

1. Introduction

The prevalence of type 2 diabetes has dramatically increased over the past 25 years, and has been predicted to maintain this expansion over the next two decades (Wild *et al.*, 2004). Although causal mechanisms remain to be elucidated, the development of insulin resistance assumes a key, early role in the pathogenesis of most cases of diabetes (Haffner *et al.*, 1990; Lillioja *et al.*, 1987; Warram *et al.*, 1990). Elevated, fasting plasma fatty acid concentrations are a hallmark of insulin resistance in obese and diabetic individuals (Boden and Shulman, 2002), and an inverse relationship between insulin sensitivity and circulating fatty acid levels has also been observed in normal-weight offspring of type 2 diabetic patients (Perseghin *et al.*, 1997). Skeletal muscle triglyceride (TG) content, estimated from biopsy samples, was found to be negatively correlated with insulin sensitivity (Pan *et al.*, 1997) and more recently, several studies have demonstrated an even stronger association with intramyocellular lipid (IMCL) content, estimated using magnetic resonance (MR) techniques (Krssak *et al.*, 1999; Perseghin *et al.*, 1999; Szczepaniak *et al.*, 1999), in healthy, as well as insulin resistant individuals. This relationship is conserved in other insulin-responsive tissues, for example, liver (Petersen *et al.*, 2002, 2005; Seppala-Lindroos *et al.*, 2002), suggesting that dysregulation of lipid metabolism may contribute to insulin resistance in these individuals. Substantiated by numerous animal studies, mechanisms for lipid-induced insulin resistance have been proposed (Morino *et al.*, 2006; Savage *et al.*, 2007; Shulman, 2000), that attribute impaired insulin action in muscle and liver to the presence of

lipid intermediates, in particular diacylglycerol (DAG), rather than intracellular TG *per se*, which interfere with the insulin-signaling cascade.

1.1. Mitochondrial fatty acid oxidation and insulin resistance

The net accumulation of intracellular lipid metabolites in muscle could either be caused by increased delivery and uptake of fatty acids, by decreased utilization, or a combination of these factors (Shulman, 2000). Intriguingly, a number of muscle biopsy studies demonstrated that the occurrence of obesity and/or diabetes was accompanied by a decrease in the content and activity of mitochondrial enzymes (Colberg *et al.*, 1995; He *et al.*, 2001; Kelley *et al.*, 1999; Ritov *et al.*, 2005; Simoneau and Kelley, 1997; Simoneau *et al.*, 1999) suggesting that impaired fatty acid oxidation may contribute to the pathogenesis of these conditions. Mitochondrial density was also found to be reduced in the muscle of obese and type 2 diabetics accompanied by smaller and morphologically damaged mitochondria (Kelley *et al.*, 2002) and analysis of gene-chip datasets indicated that down-regulation of genes associated with oxidative metabolism may occur in a coordinate manner in obese, type 2 diabetic individuals (Mootha *et al.*, 2003; Patti *et al.*, 2003) and overweight, nondiabetic subjects with a family history of diabetes (Mootha *et al.*, 2003; Patti *et al.*, 2003). However, one limitation of these muscle biopsy studies is that they provide an index of mitochondrial capacity but may not represent function. We therefore sought to implement techniques by which muscle mitochondrial function could be determined *in vivo*.

2. *In Vivo* Magnetic Resonance Spectroscopy

Since its initial demonstration as a viable methodology for *in vivo* research (Hoult *et al.*, 1974), Magnetic resonance spectroscopy (MRS) has emerged as a powerful technique for studying metabolic function in a variety of tissues in both animals and humans (Dobbins and Malloy, 2003; Prompers *et al.*, 2006; Shulman *et al.*, 1996). MRS is a companion technique to the more familiar magnetic resonance imaging (MRI) scan, which is in widespread use providing clinical anatomical images. Unlike MRI, which measures the spatial distribution of water in the region of interest, MRS determines the content of MR visible nuclei. Isotopes of many biologically relevant elements are MR visible, including hydrogen, carbon, and phosphorus. Each has a characteristic resonance frequency in the presence of a strong static magnetic field, i.e., within the MR scanner. What makes MRS of particular utility is that the chemical environment of a nucleus also influences its precise frequency, a phenomenon which gives rise to the MRS spectrum. Therefore, within a tissue of interest, the content of specific compounds and their constituent chemical groups can be resolved and determined using *in vivo* MRS. Figure 21.1 illustrates examples of *in vivo* spectra obtained from muscle showing two nuclei of metabolic relevance, phosphorus (^{31}P) and carbon (^{13}C).

The advantages of MRS as a tool for investigating muscle metabolism are considerable. It is safe, noninvasive, involves no ionizing radiation and permits repeated measures of metabolites during a single session, or over an extensive study. It is, therefore, ideal for monitoring dynamic metabolic processes. Multinuclear capabilities enable a plethora of information to be collected and provide the flexibility to study independent parameters of metabolism during the same experiment. However, MRS is a relatively insensitive technique compared to other imaging/spectrometry modalities, for example, PET (Positron Emission Tomography) or mass spectrometry, and metabolite concentrations in the millimolar range are required to be observed *in vivo*. Specialized equipment is necessary, although spectroscopy packages are now available for the new generation of clinical MR scanners.

As can be seen in panel A, a ^{31}P spectrum obtained from muscle is characterized by peaks due to phosphocreatine (PCr), the three (α, β, and γ) phosphate moieties of adenosine tri-phosphate (ATP), unbound inorganic phosphate, and mono- and di-phosphoesters (PME,

PDE). With the exception of adenosine di-phosphate (ADP), which is present in too low a concentration to be observed in resting muscle, the principal metabolites involved in energy transduction can be observed which makes *in vivo* ^{31}P MRS particularly useful for studying muscle energetics.

Since all organic compounds contain carbon atoms, ^{13}C MRS can provide information on a huge number of compounds involved in muscle metabolism. High resolution ^{13}C spectra of muscle extracts contain a myriad of overlapping peaks corresponding to different metabolites and their constituent carbons. *In vivo*, this situation is somewhat simplified, due to the low natural abundance of ^{13}C (1.1% of total carbon) and the high concentration of lipids compared to other metabolites. An *in vivo* muscle ^{13}C spectrum (Fig. 21.1B) is dominated by peaks due to the fatty acid and glycerol components of lipid, accompanied by peaks of other metabolites present in relatively high concentrations. However, this potential drawback can be turned to an advantage by infusing a ^{13}C-labeled compound and using ^{13}C MRS to monitor the metabolism of this tracer.

This article focuses on two techniques we have developed which take advantage of the unique characteristics of ^{31}P and ^{13}C MRS to investigate different facets of human muscle mitochondrial metabolism. The terminal stage of mitochondrial energy production can be estimated by using a ^{31}P magnetization-transfer technique to determine the unidirectional flux of $P_i \rightarrow$ ATP ("ATP synthesis"), and oxidation via the TCA cycle can be assessed by applying a metabolic model to ^{13}C MRS data obtained during the oxidation of a ^{13}C-labeled substrate. After providing a thorough description of the implementation of the techniques, we will describe how these parameters of muscle metabolism are modulated in insulin resistant and endurance trained individuals.

2.1. Examining exchange reactions by magnetization-transfer MRS

Although ATP can be synthesized from several sources, the principal synthetic reaction is from the combination of ADP and P_i which occurs primarily in mitochondria. ATP synthesis is in equilibrium with ATP hydrolysis as shown in Eq. (21.1), forming a phosphate exchange reaction with forward and reverse rate constants, k_f and k_r. The rate of ATP synthesis (V_{ATP}) is therefore equivalent to the forward rate constant multiplied by the concentrations of ADP and P_i, Eq. (21.2). Under steady-state conditions, where the concentration of ADP can be assumed to remain constant, this relationship can be further simplified such that V_{ATP} is the product of the pseudo-first-order rate constant (for P_i), k_f', and the P_i concentration, Eq. (21.3).

$$\mathrm{ADP} + \mathrm{P_i} \underset{k_r}{\overset{k_f}{\rightleftarrows}} \mathrm{ATP} \tag{21.1}$$

$$V_{ATP} = k_f [\mathrm{ADP}] [\mathrm{P_i}] \tag{21.2}$$

$$V_{ATP} = k_f' [\mathrm{P_i}] \tag{21.3}$$

The unidirectional fluxes involved in an exchange reaction can be studied using MRS since the magnetic equilibrium of the participant metabolites can be perturbed and monitored, while the chemical equilibrium remains intact. This effect can be accomplished using magnetization-transfer techniques (Forsen and Hoffman, 1963; Hoffman and Forsén, 1966).

As mentioned above, a ^{31}P MRS spectrum detects signals from the "high-energy phosphates" involved in cellular energetics. Therefore, the ATP synthesis flux ($P_i \rightarrow$ ATP) can be estimated, since both the ATP and P_i metabolite pools are visible.

During an MRS experiment, the signal of a particular metabolite can be expressed using the Bloch equations (Bloch, 1946), which describe the variation of the MRS signal over time. These can be modified to incorporate chemical exchange (McConnell, 1958). The response of the P_i signal involved in $P_i \leftrightarrow$ ATP exchange is shown in Eq. (21.4):

$$\mathrm{d}M_{\mathrm{Pi}}/\mathrm{d}t = \left(M_0^{\mathrm{Pi}} - M_{\mathrm{Pi}}\right)/T_1^{\mathrm{Pi}} - k_{\mathrm{f}}'\left[M_{\mathrm{Pi}}\right] + k_{\mathrm{r}}\left[M_{\mathrm{ATP}}\right] \tag{21.4}$$

where M_{Pi} is the P_i magnetization, M_0^{Pi} is the equilibrium P_i magnetization, M_{ATP} is the γ-ATP magnetization, and T_1^{Pi} is the longitudinal relaxation time of P_i.

During a magnetization-transfer experiment, the γ-phosphate peak of ATP (i.e., that which participates in exchange) can be selectively irradiated using a long-duration, frequency-selective, saturation pulse to equalize its spin-states and eliminate its signal, i.e., $M_{\mathrm{ATP}} = 0$, which simplifies the Bloch equation to Eq. (21.5).

$$\mathrm{d}M_{\mathrm{Pi}}/\mathrm{d}t = \left(M_0^{\mathrm{Pi}} - M_{\mathrm{Pi}}\right)/T_1^{\mathrm{Pi}} - k_{\mathrm{f}}'\left[M_{\mathrm{Pi}}\right] \tag{21.5}$$

Effectively this states that under conditions of γ-ATP saturation, the signal of P_i will decrease due to $P_i \rightarrow$ ATP flux. A solution to this equation is, Eq. (21.6):

$$M_{\mathrm{Pi}}' = M_0^{\mathrm{Pi}}/\left(1 + k_{\mathrm{f}}' T_1^{\mathrm{Pi}}\right) - M_0^{\mathrm{Pi}}\left\{1 - 1/\left(1 + k_{\mathrm{f}}' T_1^{\mathrm{Pi}}\right)\right\}\exp\left\{-\left(k_{\mathrm{f}}' + 1/T_1^{\mathrm{Pi}}\right)t\right\} \tag{21.6}$$

Steady-state saturation is attained following a long duration saturation pulse. Under these conditions $t \rightarrow \infty$, the second term in Eq. (21.6) vanishes, and it simplifies to:

$$M_{\mathrm{Pi}}' = M_0^{\mathrm{Pi}}/\left(1 + k_{\mathrm{f}}' T_1^{\mathrm{Pi}}\right) \tag{21.7}$$

The T_1 relaxation times of P_i under γ-ATP saturated (T_1') and non-saturated $\left(T_1^{\mathrm{Pi}}\right)$ conditions are related by the expression: $1/T_1' = 1/T_1^{\mathrm{Pi}} + k_{\mathrm{f}}'$. Substitution into Eq. (21.7) and rearranging gives the classic equation of saturation transfer, Eq. (21.8).

$$k_{\mathrm{f}}' = \left(1 - M_{\mathrm{Pi}}'/M_0^{\mathrm{Pi}}\right)/T_1' \tag{21.8}$$

Therefore, the pseudo-first-order rate constant for ATP synthesis is equivalent to the change in the P_i signal from equilibrium conditions (without saturation, M_0^{Pi}) to γ-ATP saturated conditions (M_{Pi}') expressed in units of the T_1 of P_i under conditions of γ-ATP saturation (T_1').

2.2. Measuring muscle ATP synthesis *in vivo* by ^{31}P saturation-transfer MRS

The application of the ^{31}P saturation-transfer technique to a biological system was initially used to measure the kinetics of the bacterial ATPase (Brown *et al.*, 1977), and has since

been implemented in a variety of *in vitro* and *in vivo* systems (Alger *et al.*, 1982; Brindle *et al.*, 1989; Lei *et al.*, 2003; Matthews *et al.*, 1981). We have successfully used the technique to investigate the synthesis of ATP in resting human muscle using 2.1 T and 4 T whole-body MR systems. Experimentally, our methodology incorporates three separate elements: (1) calculation of the saturation-transfer effect (i.e., M'_{Pi}/M_0^{Pi}) caused by γ-ATP saturation on P_i; (2) calibration of the T_1 of P_i under conditions of γ-ATP saturation (i.e., T'_1), together these parameters can be inserted into Eq. (21.8) to derive the rate constant for ATP synthesis; and (3) determination of the *in vivo* P_i concentration (i.e., $[P_i]$), which enables the unidirectional $P_i \rightarrow$ ATP flux to be calculated by solving Eq. (21.3).

The saturation-transfer effect can be determined by using a simple pulse-acquire MRS sequence preceded by a long, low power, frequency-selective saturation pulse (Fig. 21.2A). *In vivo*, muscle ^{31}P spectra are typically acquired using surface coils, therefore, adiabatic (B_1 insensitive) pulses are preferred for optimal signal excitation (de Graaf, 2008). Pairs of spectra are acquired with the saturation pulse centered on the γ-ATP resonance or at a downfield frequency equidistant from P_i, to partially compensate for off-resonance effects of the saturation pulse, which can be significant, particularly at lower field strengths (Kingsley and Monahan, 2000a,b). Precise acquisition parameters are system dependent; at 4 T, we use a 9 cm surface coil for ^{31}P spectroscopy of the soleus/gastrocnemius muscle complex, an adiabatic half passage (90°) pulse for excitation and a 15 s “soft” pulse for saturation. A typical pair of saturation-transfer spectra acquired with these parameters is shown in Fig. 21.3. The T_1 of P_i under conditions of γ-ATP saturation is measured by an 8-point inversion-recovery calibration using a customized sequence (Fig. 21.2B), with γ-ATP saturation not only prior to the adiabatic full passage (180°) inversion pulse, but also during the variable inversion delay to maintain steady-state saturation of the γ-ATP spins. Inversion recovery data is fitted by a 3-parameter model (MacFall *et al.*, 1987), optimized using a nonlinear least squares algorithm. A fully relaxed ^{31}P spectrum acquired without saturation is used to determine intracellular $[P_i]$, assuming a constant muscle ATP concentration of 5.5 mmol/kg (Kemp *et al.*, 2007).

2.3. Monitoring metabolic fluxes using ^{13}C MRS

As mentioned previously, ^{13}C MRS offers a method to examine the metabolism of carbon-based compounds *in vivo*. The metabolic fate of a ^{13}C-labeled substrate can be monitored in real time, providing that it is metabolized sufficiently rapidly to induce a significant, dynamic enrichment in one of its metabolic products, that this product can be resolved from other metabolites with ^{13}C MRS and that it is of high enough concentration to be detected *in vivo*. For mitochondrial metabolism, the TCA cycle, which participates in the oxidation of lipids and carbohydrate, is ideally suited for examination by this technique.

Substrates derived from either source enter the cycle via the common intermediate, acetyl CoA, and are metabolized through a series of condensation, isomerization and oxidation (decarboxylation) reactions in the mitochondrial matrix ultimately producing carbon dioxide, NADH and $FADH_2$, the latter of which are oxidized by the electron transport chain. The ^{13}C label can be introduced into the cycle as shown in Fig. 21.4 by infusing [2-^{13}C]-labeled acetate as an MR-visible tracer, which is rapidly taken up by muscle and other tissues and converted into [2-^{13}C]-acetyl-CoA that enters the TCA cycle by condensing with oxaloacetate to form [4-^{13}C]-citrate. The position of the ^{13}C label is conserved through the initial steps of the TCA cycle, labeling α-ketoglutarate at the C_4 position. The principal TCA-cycle intermediates (TCAI) are present in concentrations that are too low to be observed *in vivo* using ^{13}C MRS. However, glutamate, which is present in millimolar concentrations in muscle, is in relatively rapid exchange with α-ketoglutarate and will also become ^{13}C enriched at C_4. As the TCA cycle progresses, the ^{13}C label becomes scrambled

between the C_2 and C_3 positions due to the symmetry of the succinate molecule; a second turn of the TCA cycle yields [2-^{13}C] and [3–^{13}C]-glutamate.

Unlike brain, where natural abundance [4-^{13}C]-glutamate can be resolved in an *in vivo* ^{13}C MRS spectra, the C_4 glutamate peak at 34.3 ppm in muscle is obscured by overlapping lipid resonances as shown in Fig. 21.1. The contribution from sub-cutaneous fat can be eliminated by using a localized MRS sequence to selectively acquire signal from muscle only. The IMCL contribution is also significant, but can be minimized by an inversion-null strategy which takes advantage of the more rapid T_1 relaxation times of lipid moieties compared to other metabolites as shown in Fig. 21.5. At 4 T, we use an adiabatic ^{1}H–^{13}C polarization-transfer (PT) sequence (Burum and Ernst, 1980; Shen *et al.*, 1999) for ^{13}C acquisition with WALTZ 16 decoupling. PT echo-times are optimized for C_4 glutamate detection. Spectra are acquired using a 9 cm diameter ^{13}C surface coil positioned underneath the soleus-gastrocnemius muscle complex of the calf, with twin, orthogonal 13 cm diameter ^{1}H surface coils arrayed in quadrature for decoupling and excitation/inversion on the ^{1}H channel. Voxel localization is achieved using 2-dimensional outer volume suppression (OVS) to select a ~90 cm^3 volume within the calf muscles. OVS enables the maximal ^{13}C metabolite signal to be acquired, although an ISIS-based localization scheme could also be implemented. IMCL is suppressed using adiabatic T_1-selective nulling, as described above, optimized for the lipid resonance at 34.7 ppm. Previously, we have used direct ^{13}C detection with decoupling at 2.1 T (Lebon *et al.*, 2001); however, the acquired ^{13}C signal is enhanced approximately 2-fold *in vivo* by using a PT sequence, and localization and lipid suppression can be performed on the ^{1}H channel where there is less error due to chemical shift dispersion.

To determine the TCA cycle flux, the time course of ^{13}C incorporation into C_4-glutamate is monitored during a 120-min infusion of 99% enriched [2-^{13}C]-acetate (350 mmol/l sodium salt) at a rate of 3.0 mg/kg/min. ^{13}C spectra are acquired with ~5 min time resolution for 20 min prior to the infusion to establish a baseline, and continuously until the end of the experiment. Plasma samples are obtained at 10 min intervals throughout the experiment for the measurement of plasma acetate concentration and fractional enrichment by gas chromatography/mass spectrometry (Befroy *et al.*, 2007). Steady-state enrichment of plasma acetate is attained within 5 min of originating the infusion and reaches ~85%; with the concentration of plasma acetate approximately 0.80 m*M*, consistent with functioning as a tracer-level substrate. To eliminate any residual contribution of lipid, the increment in the C_4-glutamate peak during the infusion is determined from difference spectra created by subtracting averaged baseline spectra from the ^{13}C spectrum for each time-point. The maximal enrichment in the [4-^{13}C]-glutamate peak is calculated relative to that of the C_2-glutamate peak assuming partial (5%) dilution of the C_2 pool due to anaplerosis. The absolute enrichment of the C_2-glutamate peak at the end of infusion is determined relative to the natural abundance enrichment (1.1%) of the baseline spectra.

2.4. Metabolic modeling of the TCA cycle flux

The TCA cycle flux (V_{TCA}) is determined by using CWave software to model the incorporation of ^{13}C label from plasma [2-^{13}C]-acetate into the muscle [4-^{13}C]-glutamate pool. The CWave model consists of isotopic mass balance equations shown below that describe the metabolic fate of the plasma [2-^{13}C]-acetate. The corresponding reaction rates are noted in Fig. 21.4. The ^{13}C label enters the TCA cycle following the conversion of [2-^{13}C]-acetate into [2-^{13}C]-acetylCoA (V_{AC}). Entry of unlabeled substrates via acetyl CoA is incorporated into the model as a separate reaction ($V_{PDH + FA}$). CWave determines V_{TCA} as the rate of total carbon flow from acetyl CoA to α-ketoglutarate using a non-linear least-squares algorithm to fit the curve of C_4-glutamate enrichment. The rate of α-ketoglutarate/glutamate exchange has been determined in previous studies and is fixed at 150 nmol/g(muscle)/min which is significantly faster than the TCA cycle flux, and therefore non-

limiting. In this model, V_{TCA} is equal to the sum of (V_{AC} + V_{PDH+FA}) but is independent of the absolute fractional enrichment at C_4-glutamate (V_{AC}/V_{PDH+FA}). The intracellular concentration of glutamate has been determined by enzymatic analysis of muscle biopsy samples from healthy individuals, and is assumed to be 2.41 mmol/l in all subject groups (Lebon *et al.*,2001). In our *in vivo* studies to date, the ratio of natural abundance C_2-glutamate/C_2-creatine is unaffected by the study population indicating that the intracellular concentration of glutamate is stable (Befroy *et al.*, 2007, 2008a). The concentrations of the other TCAI are very low and therefore not critical to the accuracy of the model and have been taken from the literature (Hawkins and Mans, 1983). The curve of muscle [4-^{13}C]-glutamate enrichment for a typical healthy individual is shown in Fig. 21.6 with the fit of the CWave metabolic model of these data superimposed, along with the calculated V_{TCA}.

2.4.1. Isotopic mass balance equations

2.4.1.1. Mass balance:

$$\begin{aligned}
&\mathrm{d(Citrate)}/\mathrm{d}t = V_{TCA} - V_{TCA}\\
&\mathrm{d}(\alpha\mathrm{KG})/\mathrm{d}t = V_{TCA} + V_X - (V_{TCA} + V_X)\\
&\mathrm{d(Glutamate)}/\mathrm{d}t = V_X - V_X\\
&\mathrm{d(AcetylCoA)}/\mathrm{d}t = V_{AC} + V_{PDH+FA} - V_{TCA}
\end{aligned}$$

2.4.1.2. Isotope balance:

$$\begin{aligned}
\mathrm{d}(C_4\text{–Citrate})/\mathrm{d}t &= V_{TCA}\,(C_2\text{–AcetylCoA/AcetylCoA}) - V_{TCA}\,(C_4\text{–Citrate/Citrate})\\
\mathrm{d}(C_4\text{–}\alpha\mathrm{KG})/\mathrm{d}t &= V_{TCA}\,(C_4\text{–Citrate/Citrate}) + V_X\,(C_4\text{–Glutamate/Glutamate}) - (V_{TCA} + V_X)\,(C_4\text{–}\alpha\mathrm{KG}/\alpha\mathrm{KG})\\
\mathrm{d}(C_4\text{–Glutamate})/\mathrm{d}t &= V_X\,(C_4\text{–}\alpha\mathrm{KG}/\alpha\mathrm{KG}) - V_X\,(C_4\text{–Glutamate/Glutamate})\\
\mathrm{d}(C_2\text{–AcetylCoA})/\mathrm{d}t &= V_{AC}\,(C_2\text{–Acetate/Acetate}) + V_{PDH+FA}\,(C_0\text{–FFA/FFA}) - V_{TCA}\,(C_2\text{–AcetylCoA/AcetylCoA})
\end{aligned}$$

2.4.1.3. Muscle metabolite concentrations:

$$\begin{aligned}
\mathrm{AcetylCoA} &= 0.05 \quad \mathrm{umol/g}\\
\mathrm{Citrate} &= 0.02 \quad \mathrm{umol/g}\\
\mathrm{Glutamate} &= 2.41 \quad \mathrm{umol/g}\\
\alpha\mathrm{KG} &= 0.05 \quad \mathrm{umol/g}
\end{aligned}$$

This relatively simple metabolic model, which incorporates only a single turn of the TCA cycle, and requires only plasma C_2-acetate and muscle C_4-glutamate enrichment, performs well in resting muscle. The advantage of the single-turn model is that the ^{13}C MRS methods can be optimized to detect [4-^{13}C]-glutamate with the maximum possible sensitivity and time-resolution and therefore obtain the most accurate time course of enrichment. This scheme generates the same rates of V_{TCA} as a more robust 2-turn model that also requires data for muscle C_2-glutamate which is enriched during a second turn of the TCA cycle. We have previously used this more complex model to estimate V_X which confirmed our assumption that $V_X > V_{TCA}$ (Befroy *et al.*, 2007; Lebon *et al.*, 2001). We also investigated the influence of anaplerosis on the calculated rate of TCA cycle flux by using a model that incorporated an anaplerotic flux via pyruvate carboxylase (V_{ana}). The calculated V_{TCA} is unaffected by incremental increases in V_{ana} up to 20% of V_{TCA} (Befroy *et al.*, 2007), which is significantly greater than is likely in resting muscle. We have also found that the absolute fractional enrichment of C_2-glutamate at the end of the [2-^{13}C]-acetate infusion is not different between subject groups in our studies, indicating that rates of anaplerosis in

quiescent muscle are similar between study populations (Befroy *et al.*, 2007, 2008a). However, this condition may not be preserved for all subject cohorts or in other tissues.

3. Insulin Resistance and Resting Mitochondrial Metabolism

Using the techniques outlined above, we have examined how these parameters of resting mitochondrial metabolism are affected in two different cohorts of insulin-resistant individuals. Both V_{TCA} and V_{ATP} were decreased by ~40% in the muscle of insulin-resistant elderly subjects (mean age ~70 years) compared with activity-matched young adults (mean age ~27 years) (Petersen *et al.*, 2003), demonstrating that these older individuals had decreased resting mitochondrial function. Similarly, both parameters were decreased ~30% in insulin-resistant offspring of type 2 diabetic patients compared with insulin-sensitive controls (Befroy *et al.*, 2007; Petersen et al., 2004), consistent with the ~40% reduced mitochondrial density observed in a similar cohort of subjects (Morino *et al.*, 2005). Average curves of muscle [4-^{13}C]-glutamate enrichment for each group are shown in Fig. 21.7, with the fits of the CWave model superimposed, demonstrating the difference in the rates of enrichment and the resultant TCA cycle flux between these cohorts. It is worth noting that these studies were performed in lean, otherwise healthy individuals and the subject groups were matched for body composition, to prevent the confounding factor of obesity, and to try to isolate effects occurring early in the pathogenesis of insulin resistance. Activity levels were also matched, since many of the age-related effects on muscle metabolism can be attributed to the decrease in physical activity that typically occurs in older individuals (Chilibeck *et al.*, 1998; Kent-Braun and Ng, 2000). These spectroscopy techniques are also independent of the mass of tissue from which the MRS signal is detected and are therefore not directly affected by the muscle atrophy that is commonly associated with aging (Frontera *et al.*, 1991).

We have also investigated how resting mitochondrial metabolism is modulated in endurance trained muscle, which is characterized by increased mitochondrial number and content of oxidative enzymes. Although V_{TCA} was increased in the muscle of trained individuals, V_{ATP} was unaltered (Befroy *et al.*, 2008a) suggesting a decrease in the efficiency of energy production at rest. This elevated “idling” rate of the mitochondria may enable a more rapid response to the increased energy demand at the onset of exercise. We did not observe any significant effect on whole-body energy expenditure demonstrating that whole-body indirect calorimetry techniques are too insensitive to detect significant changes in muscle oxidation rates.

Comparison of the absolute rates of V_{ATP}, calculated by the ^{31}P-saturation-transfer technique, and of oxygen consumption, estimated by a number of techniques (including V_{TCA} by ^{13}C MRS), give rise to P:O ratios in resting muscle which are higher than the theoretical maximum (Brindle *et al.*, 1989; Kemp, 2008). This is in contrast to other tissues which have higher respiration rates, for example, kidney (Freeman *et al.*, 1983) and brain (Du *et al.*, 2008; Lei *et al.*, 2003), where good agreement is observed between these parameters. The total $P_i \rightarrow ATP$ flux from all cellular contributions (oxidative + glycolytic) is evaluated using the saturation-transfer technique; although the glycolytic contribution in resting muscle is low (Jucker *et al.*, 2000); and unpublished data) it has been postulated that in quiescent muscle reversible $P_i \rightarrow ATP$ exchange via the mitochondrial F_1F_0 ATPase may contribute to the elevated absolute V_{ATP} (Brindle and Radda, 1987; Campbell-Burk *et al.*, 1987). It is worth noting that even if exchange is the dominating contribution, it is likely to be proportional to the F_1 ATPase activity. We have successfully miniaturized the saturation-transfer technique to study mouse muscle and have found that the $P_i \rightarrow ATP$ flux responds as expected to perturbations in the expression of mitochondrial genes in transgenic mice including UCP3 knock-out (Cline *et al.*, 2001) and UCP3 overexpression (Befroy

unpublished data) and PGC1α overexpression (Choi *et al.*, 2008) confirming that the rate of ATP synthesis determined by the saturation-transfer technique is an effective biomarker of mitochondrial function.

3.1. Resting mitochondrial metabolism versus maximal capacity

In counterpoint to our *in vivo* MRS studies investigating resting muscle mitochondrial metabolism, other groups have observed that mitochondrial oxidative capacity, estimated *in vivo* from PCr kinetics during exercise, was unaffected by aging (Chilibeck *et al.*, 1998; Lanza *et al.*, 2005) when activity patterns were accounted for, and was unchanged throughout the development of insulin-resistance and diabetes in the ZDF rat (De Feyter *et al.*, 2008). Muscle biopsy studies also suggest that mitochondrial capacity is increased in Asian-Indians despite severe insulin resistance (Nair *et al.*, 2008). The disparity between these studies highlights the fact that capacity and resting function are different parameters of mitochondrial metabolism, likely to be regulated or limited by different factors, and that the term mitochondrial “dysfunction,” which has become commonly used in the field and the source of some controversy, is misleading since it has no precise definition and could refer to reduced capacity, function or a combination of both. Furthermore, the findings of these studies will also have been influenced by the precise characteristics of the populations studied and the muscle chosen for analysis. Different muscle groups exhibit distinct metabolic and functional phenotypes (Essen *et al.*, 1975; Pette and Spamer, 1986) and respond differently to aging (Houmard *et al.*, 1998) and potentially disease. Therefore, it is highly likely that there are muscle-group specific differences in mitochondrial function and capacity in healthy subjects and in the modulation of energy production by aging/disease. With this issue in mind, we have recently implemented the saturation-transfer methodology in a localized manner to obtain muscle-group specific rates of $P_i \rightarrow$ ATP flux (Befroy *et al.*, 2008b).

4. Conclusions

Because of its distinct characteristics, MRS is a unique tool for investigating metabolism across a wide range of systems, encompassing human, animal and cellular models, a wide array of tissues, and *in vivo* as well as *in vitro* applications. Multinuclear capabilities further extend these possibilities and since the technique is non-invasive, dynamic processes can be studied using repeated measurements in addition to static estimates of metabolite concentrations. By taking advantage of these unique properties, we have developed techniques that allow us to monitor muscle mitochondrial metabolism *in vivo* and investigate how it is modulated in health and disease. The implementation of spectroscopy packages on clinical MR scanners will allow these methodologies to reach a wider audience of investigators. With the progression to higher-field MR systems, which increase spectral resolution and sensitivity, and the continued development of enhanced detection techniques, there are a multitude of possibilities for future research.

REFERENCES

Alger JR, den Hollander JA, Shulman RG. *In vivo* phosphorus-31 nuclear magnetic resonance saturation transfer studies of adenosinetriphosphatase kinetics in Saccharomyces cerevisiae. Biochemistry. 1982; 21:2957–2963. [PubMed: 6213261]

Befroy DE, Petersen KF, Dufour S, Mason GF, de Graaf RA, Rothman DL, Shulman GI. Impaired mitochondrial substrate oxidation in muscle of insulin-resistant offspring of type 2 diabetic patients. Diabetes. 2007; 56:1376–1381. [PubMed: 17287462]

Befroy DE, Petersen KF, Dufour S, Mason GF, Rothman DL, Shulman GI. Increased substrate oxidation and mitochondrial uncoupling in skeletal muscle of endurance-trained individuals. Proc. Natl. Acad. Sci. USA. 2008a; 105:16701–16706. [PubMed: 18936488]

Befroy DE, Petersen KF, Shulman GI, Rothman DL. Localized 31P saturation transfer reveals differences in gastrocnemius and soleus rates of ATP synthesis in-vivo. Proc. Int. Soc. Mag. Reson. Med. 2008b:2565.

Bloch F. Nuclear induction. Phys. Rev. 1946; 70:460.

Boden G, Shulman GI. Free fatty acids in obesity and type 2 diabetes: Defining their role in the development of insulin resistance and beta-cell dysfunction. Eur. J. Clin. Invest. 2002; 32(Suppl. 3): 14–23. [PubMed: 12028371]

Brindle KM, Blackledge MJ, Challiss RA, Radda GK. ^{31}P NMR magnetization-transfer measurements of ATP turnover during steady-state isometric muscle contraction in the rat hind limb *in vivo*. Biochemistry. 1989; 28:4887–4893. [PubMed: 2765517]

Brindle KM, Radda GK. ^{31}P-NMR saturation transfer measurements of exchange between Pi and ATP in the reactions catalysed by glyceraldehyde-3-phosphate dehydrogenase and phosphoglycerate kinase *in vitro*. Biochim. Biophys. Acta. 1987; 928:45–55. [PubMed: 3828401]

Brown TR, Ugurbil K, Shulman RG. ^{31}P nuclear magnetic resonance measurements of ATPase kinetics in aerobic Escherichia coli cells. Proc. Natl. Acad. Sci. USA. 1977; 74:5551–5553. [PubMed: 146199]

Burum DP, Ernst RR. Net polarization transfer via a J-ordered state for signal enhancement of low-sensitivity nuclei. J. Magn. Reson. 1980; 39:163–168. 1969.

Campbell-Burk SL, Jones KA, Shulman RG. ^{31}P NMR saturation-transfer measurements in Saccharomyces cerevisiae: Characterization of phosphate exchange reactions by iodoacetate and antimycin A inhibition. Biochemistry. 1987; 26:7483–7492. [PubMed: 3322400]

Chilibeck PD, McCreary CR, Marsh GD, Paterson DH, Noble EG, Taylor AW, Thompson RT. Evaluation of muscle oxidative potential by ^{31}P-MRS during incremental exercise in old and young humans. Eur. J. Appl. Physiol. Occup. Physiol. 1998; 78:460–465. [PubMed: 9809848]

Choi CS, Befroy DE, Codella R, Kim S, Reznick RM, Hwang Y, Liu Z, Lee H, Distefano A, Samuel VT, Zhang D, Cline GW, et al. Paradoxical effects of increased expression of PGC-1α on muscle mitochondrial function and insulin-stimulated muscle glucose metabolism. Proc. Natl. Acad. Sci. USA. 2008; 105:19926–19931. [PubMed: 19066218]

Cline GW, Vidal-Puig AJ, Dufour S, Cadman KS, Lowell BB, Shulman GI. *In vivo* effects of uncoupling protein-3 gene disruption on mitochondrial energy metabolism. J. Biol. Chem. 2001; 276:20240–20244. [PubMed: 11274222]

Colberg SR, Simoneau JA, Thaete FL, Kelley DE. Skeletal muscle utilization of free fatty acids in women with visceral obesity. J. Clin. Invest. 1995; 95:1846–1853. [PubMed: 7706491]

De Feyter HM, Lenaers E, Houten SM, Schrauwen P, Hesselink MK, Wanders RJ, Nicolay K, Prompers JJ. Increased intramyocellular lipid content but normal skeletal muscle mitochondrial oxidative capacity throughout the pathogenesis of type 2 diabetes. FASEB J. 2008; 22:3947–3955. [PubMed: 18653763]

de Graaf, RA. *In vivo* NMR Spectroscopy: Principles and Techniques. Wiley, Chichester: 2008.

Dobbins RL, Malloy CR. Measuring *in-vivo* metabolism using nuclear magnetic resonance. Curr. Opin. Clin. Nutr. Metab. Care. 2003; 6:501–509. [PubMed: 12913667]

Du F, Zhu XH, Zhang Y, Friedman M, Zhang N, Ugurbil K, Chen W. Tightly coupled brain activity and cerebral ATP metabolic rate. Proc. Natl. Acad. Sci. USA. 2008; 105:6409–6414. [PubMed: 18443293]

Essen B, Jansson E, Henriksson J, Taylor AW, Saltin B. Metabolic characteristics of fibre types in human skeletal muscle. Acta Physiol. Scand. 1975; 95:153–165. [PubMed: 242187]

Forsen S, Hoffman RA. Study of moderately rapid chemical exchange reactions by means of nuclear magnetic double resonance. J. Chem. Phys. 1963; 39:2892–2901.

Freeman D, Bartlett S, Radda G, Ross B. Energetics of sodium transport in the kidney. Saturation transfer ^{31}P-NMR. Biochim. Biophys. Acta. 1983; 762:325–336. [PubMed: 6830878]

Frontera WR, Hughes VA, Lutz KJ, Evans WJ. A cross-sectional study of muscle strength and mass in 45- to 78-yr-old men and women. J. Appl. Physiol. 1991; 71:644–650. [PubMed: 1938738]

Haffner SM, Stern MP, Mitchell BD, Hazuda HP, Patterson JK. Incidence of type II diabetes in Mexican Americans predicted by fasting insulin and glucose levels, obesity, and body-fat distribution. Diabetes. 1990; 39:283–288. [PubMed: 2407581]

Hawkins, RA.; Mans, AM. Intermediary metabolism of carbohydrates and other fuels. In: Lajtha, A., editor. Handbook of Neurochemistry. Vol. 3. Plenum; New York: 1983. p. 259-294.

He J, Watkins S, Kelley DE. Skeletal muscle lipid content and oxidative enzyme activity in relation to muscle fiber type in type 2 diabetes and obesity. Diabetes. 2001; 50:817–823. [PubMed: 11289047]

Hoffman RA, Forsén S. High resolution nuclear magnetic double and multiple resonance. Prog. NMR Spectrosc. 1966; 1:15–204.

Hoult DI, Busby SJ, Gadian DG, Radda GK, Richards RE, Seeley PJ. Observation of tissue metabolites using ^{31}P nuclear magnetic resonance. Nature. 1974; 252:285–287. [PubMed: 4431445]

Houmard JA, Weidner ML, Gavigan KE, Tyndall GL, Hickey MS, Alshami A. Fiber type and citrate synthase activity in the human gastrocnemius and vastus lateralis with aging. J. Appl. Physiol. 1998; 85:1337–1341. [PubMed: 9760325]

Jucker BM, Ren J, Dufour S, Cao X, Previs SF, Cadman KS, Shulman GI. ^{13}C/^{31}P NMR assessment of mitochondrial energy coupling in skeletal muscle of awake fed and fasted rats. Relationship with uncoupling protein 3 expression. J. Biol. Chem. 2000; 275:39279–39286. [PubMed: 10995775]

Kelley DE, Goodpaster B, Wing RR, Simoneau JA. Skeletal muscle fatty acid metabolism in association with insulin resistance, obesity, and weight loss. Am. J. Physiol. Endocrinol. Metab. 1999; 277:E1130–E1141.

Kelley DE, He J, Menshikova EV, Ritov VB. Dysfunction of mitochondria in human skeletal muscle in type 2 diabetes. Diabetes. 2002; 51:2944–2950. [PubMed: 12351431]

Kemp GJ. The interpretation of abnormal ^{31}P magnetic resonance saturation transfer measurements of Pi/ATP exchange in insulin-resistant skeletal muscle. Am. J. Physiol. Endocrinol. Metab. 2008; 294:E640–E642. author reply E643–E644. [PubMed: 18325881]

Kemp GJ, Meyerspeer M, Moser E. Absolute quantification of phosphorus metabolite concentrations in human muscle *in vivo* by 31P MRS: A quantitative review. NMR Biomed. 2007; 20:555–565. [PubMed: 17628042]

Kent-Braun JA, Ng AV. Skeletal muscle oxidative capacity in young and older women and men. J. Appl. Physiol. 2000; 89:1072–1078. [PubMed: 10956353]

Kingsley PB, Monahan WG. Corrections for off-resonance effects and incomplete saturation in conventional (two-site) saturation-transfer kinetic measurements. Magn. Reson. Med. 2000a; 43:810–819. [PubMed: 10861875]

Kingsley PB, Monahan WG. Effects of off-resonance irradiation, cross-relaxation, and chemical exchange on steady-state magnetization and effective spin-lattice relaxation times. J. Magn. Reson. 2000b; 143:360–375. [PubMed: 10729261]

Krssak M, Falk Petersen K, Dresner A, DiPietro L, Vogel SM, Rothman DL, Roden M, Shulman GI. Intramyocellular lipid concentrations are correlated with insulin sensitivity in humans: A ^{1}H NMR spectroscopy study. Diabetologia. 1999; 42:113–116. [PubMed: 10027589]

Lanza IR, Befroy DE, Kent-Braun JA. Age-related changes in ATP-producing pathways in human skeletal muscle *in vivo*. J. Appl. Physiol. 2005; 99:1736–1744. [PubMed: 16002769]

Lebon V, Dufour S, Petersen KF, Ren J, Jucker BM, Slezak LA, Cline GW, Rothman DL, Shulman GI. Effect of triiodothyronine on mitochondrial energy coupling in human skeletal muscle. J. Clin. Invest. 2001; 108:733–737. [PubMed: 11544279]

Lei H, Ugurbil K, Chen W. Measurement of unidirectional Pi to ATP flux in human visual cortex at 7 T by using *in vivo* ^{31}P magnetic resonance spectroscopy. Proc. Natl. Acad. Sci. USA. 2003; 100:14409–14414. [PubMed: 14612566]

Lillioja S, Young AA, Culter CL, Ivy JL, Abbott WG, Zawadzki JK, Yki-Jarvinen H, Christin L, Secomb TW, Bogardus C. Skeletal muscle capillary density and fiber type are possible determinants of *in vivo* insulin resistance in man. J. Clin. Invest. 1987; 80:415–424. [PubMed: 3301899]

MacFall JR, Wehrli FW, Breger RK, Johnson GA. Methodology for the measurement and analysis of relaxation times in proton imaging. Magn. Reson. Imaging. 1987; 5:209–220. [PubMed: 3041152]

Matthews PM, Bland JL, Gadian DG, Radda GK. The steady-state rate of ATP synthesis in the perfused rat heart measured by ^{31}P NMR saturation transfer. Biochem. Biophys. Res. Commun. 1981; 103:1052–1059. [PubMed: 7332573]

McConnell HM. Reaction rates by nuclear magnetic resonance. J. Chem. Phys. 1958; 28:430–431.

Mootha VK, Lindgren CM, Eriksson KF, Subramanian A, Sihag S, Lehar J, Puigserver P, Carlsson E, Ridderstrale M, Laurila E, Houstis N, Daly MJ, et al. PGC-1alpha-responsive genes involved in oxidative phosphorylation are coordinately downregulated in human diabetes. Nat. Genet. 2003; 34:267–273. [PubMed: 12808457]

Morino K, Petersen KF, Dufour S, Befroy D, Frattini J, Shatzkes N, Neschen S, White MF, Bilz S, Sono S, Pypaert M, Shulman GI. Reduced mitochondrial density and increased IRS-1 serine phosphorylation in muscle of insulin-resistant offspring of type 2 diabetic parents. J. Clin. Invest. 2005; 115:3587–3593. [PubMed: 16284649]

Morino K, Petersen KF, Shulman GI. Molecular mechanisms of insulin resistance in humans and their potential links with mitochondrial dysfunction. Diabetes. 2006; 55(Suppl. 2):S9–S15. [PubMed: 17130651]

Nair KS, Bigelow ML, Asmann YW, Chow LS, Coenen-Schimke JM, Klaus KA, Guo ZK, Sreekumar R, Irving BA. Asian Indians have enhanced skeletal muscle mitochondrial capacity to produce ATP in association with severe insulin resistance. Diabetes. 2008; 57:1166–1175. [PubMed: 18285554]

Pan DA, Lillioja S, Kriketos AD, Milner MR, Baur LA, Bogardus C, Jenkins AB, Storlien LH. Skeletal muscle triglyceride levels are inversely related to insulin action. Diabetes. 1997; 46:983–988. [PubMed: 9166669]

Patti ME, Butte AJ, Crunkhorn S, Cusi K, Berria R, Kashyap S, Miyazaki Y, Kohane I, Costello M, Saccone R, Landaker EJ, Goldfine AB, et al. Coordinated reduction of genes of oxidative metabolism in humans with insulin resistance and diabetes: Potential role of PGC1 and NRF1. Proc. Natl. Acad. Sci. USA. 2003; 100:8466–8471. [PubMed: 12832613]

Perseghin G, Ghosh S, Gerow K, Shulman GI. Metabolic defects in lean nondiabetic offspring of NIDDM parents: A cross-sectional study. Diabetes. 1997; 46:1001–1009. [PubMed: 9166672]

Perseghin G, Scifo P, De Cobelli F, Pagliato E, Battezzati A, Arcelloni C, Vanzulli A, Testolin G, Pozza G, Del Maschio A, Luzi L. Intramyo-cellular triglyceride content is a determinant of *in vivo* insulin resistance in humans: A ^{1}H-^{13}C nuclear magnetic resonance spectroscopy assessment in offspring of type 2 diabetic parents. Diabetes. 1999; 48:1600–1606. [PubMed: 10426379]

Petersen KF, Befroy D, Dufour S, Dziura J, Ariyan C, Rothman DL, DiPietro L, Cline GW, Shulman GI. Mitochondrial dysfunction in the elderly: Possible role in insulin resistance. Science. 2003; 300:1140–1142. [PubMed: 12750520]

Petersen KF, Dufour S, Befroy D, Garcia R, Shulman GI. Impaired mitochondrial activity in the insulin-resistant offspring of patients with type 2 diabetes. N. Engl. J. Med. 2004; 350:664–671. [PubMed: 14960743]

Petersen KF, Dufour S, Befroy D, Lehrke M, Hendler RE, Shulman GI. Reversal of nonalcoholic hepatic steatosis, hepatic insulin resistance, and hyper-glycemia by moderate weight reduction in patients with type 2 diabetes. Diabetes. 2005; 54:603–608. [PubMed: 15734833]

Petersen KF, Oral EA, Dufour S, Befroy D, Ariyan C, Yu C, Cline GW, DePaoli AM, Taylor SI, Gorden P, Shulman GI. Leptin reverses insulin resistance and hepatic steatosis in patients with severe lipodystrophy. J. Clin. Invest. 2002; 109:1345–1350. [PubMed: 12021250]

Pette D, Spamer C. Metabolic properties of muscle fibers. Fed. Proc. 1986; 45:2910–2914. [PubMed: 3536589]

Prompers JJ, Jeneson JA, Drost MR, Oomens CC, Strijkers GJ, Nicolay K. Dynamic MRS and MRI of skeletal muscle function and biomechanics. NMR Biomed. 2006; 19:927–953. [PubMed: 17075956]

Ritov VB, Menshikova EV, He J, Ferrell RE, Goodpaster BH, Kelley DE. Deficiency of subsarcolemmal mitochondria in obesity and type 2 diabetes. Diabetes. 2005; 54:8–14. [PubMed: 15616005]

Savage DB, Petersen KF, Shulman GI. Disordered lipid metabolism and the pathogenesis of insulin resistance. Physiol. Rev. 2007; 87:507–520. [PubMed: 17429039]

Seppala-Lindroos A, Vehkavaara S, Hakkinen AM, Goto T, Westerbacka J, Sovijarvi A, Halavaara J, Yki-Jarvinen H. Fat accumulation in the liver is associated with defects in insulin suppression of glucose production and serum free fatty acids independent of obesity in normal men. J. Clin. Endocrinol. Metab. 2002; 87:3023–3028. [PubMed: 12107194]

Shen J, Petersen KF, Behar KL, Brown P, Nixon TW, Mason GF, Petroff OA, Shulman GI, Shulman RG, Rothman DL. Determination of the rate of the glutamate/glutamine cycle in the human brain by *in vivo* ^{13}C NMR. Proc. Natl. Acad. Sci. USA. 1999; 96:8235–8240. [PubMed: 10393978]

Shulman GI. Cellular mechanisms of insulin resistance. J. Clin. Invest. 2000; 106:171–176. [PubMed: 10903330]

Shulman RG, Rothman DL, Price TB. Nuclear magnetic resonance studies of muscle and applications to exercise and diabetes. Diabetes. 1996; 45(Suppl. 1):S93–S98. [PubMed: 8529808]

Simoneau JA, Kelley DE. Altered glycolytic and oxidative capacities of skeletal muscle contribute to insulin resistance in NIDDM. J. Appl. Physiol. 1997; 83:166–171. [PubMed: 9216960]

Simoneau JA, Veerkamp JH, Turcotte LP, Kelley DE. Markers of capacity to utilize fatty acids in human skeletal muscle: Relation to insulin resistance and obesity and effects of weight loss. FASEB J. 1999; 13:2051–2060. [PubMed: 10544188]

Szczepaniak LS, Babcock EE, Schick F, Dobbins RL, Garg A, Burns DK, McGarry JD, Stein DT. Measurement of intracellular triglyceride stores by H spectroscopy: Validation in vivo. Am. J. Physiol. Endocrinol. Metab. 1999; 276:E977–E989.

Warram JH, Martin BC, Krolewski AS, Soeldner JS, Kahn CR. Slow glucose removal rate and hyperinsulinemia precede the development of type II diabetes in the offspring of diabetic parents. Ann. Intern. Med. 1990; 113:909–915. [PubMed: 2240915]

Wild S, Roglic G, Green A, Sicree R, King H. Global prevalence of diabetes: Estimates for the year 2000 and projections for 2030. Diabetes Care. 2004; 27:1047–1053. [PubMed: 15111519]

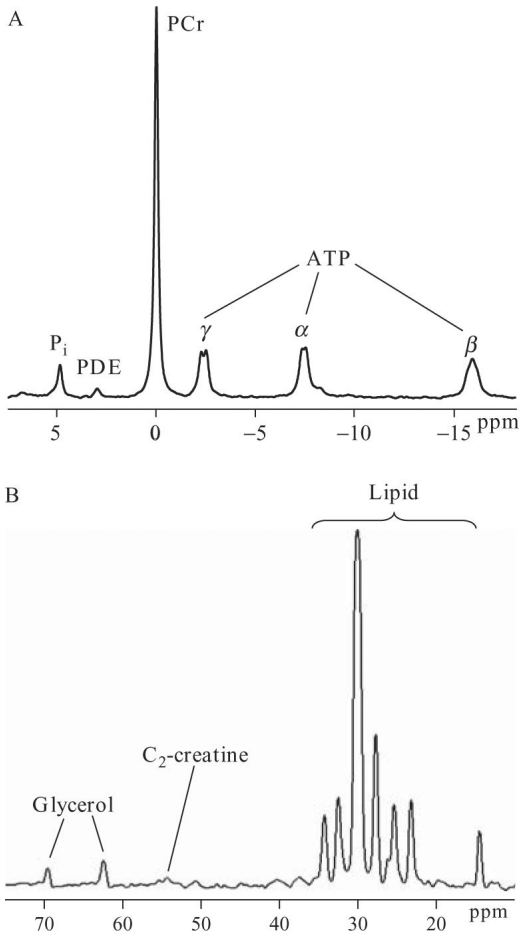

Figure 21.1.
Typical ^{31}P (A) and ^{13}C (B) MRS spectra acquired from the soleus-gastrocnemius muscle complex *in vivo*.

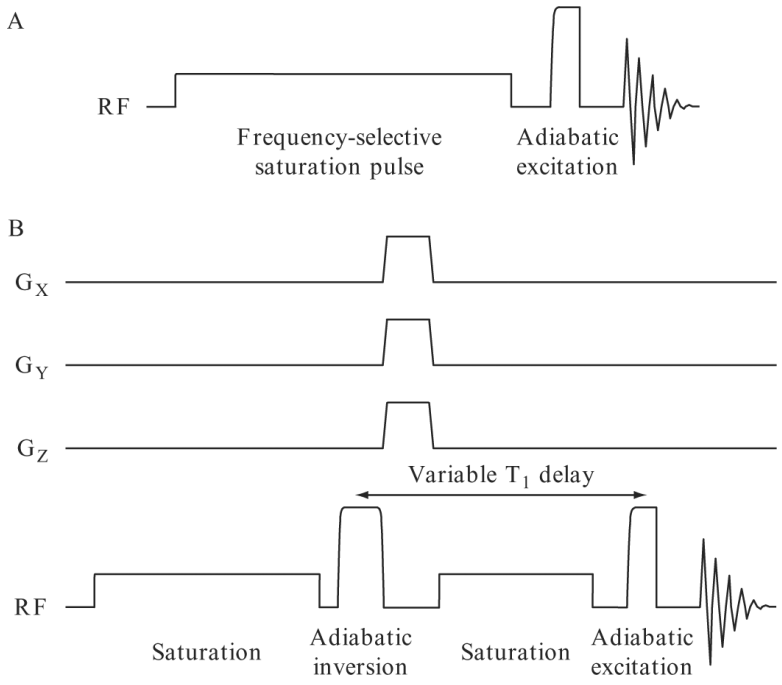

Figure 21.2.

Pulse sequences for the ^{31}P saturation-transfer experiment. (A) Pulse-acquire sequence with RF saturation. A long, low power, frequency-selective saturation pulse precedes signal excitation/detection. Adiabatic excitation pulses are optimal for *in vivo* MRS using surface coils. (B) Inversion-recovery with RF saturation for T_1' calibration. Frequency-selective saturation of the γ-ATP peak is applied prior to the adiabatic inversion pulse, and during the variable inversion-delay to maintain steady-state spin saturation throughout the inversion-recovery measurement.

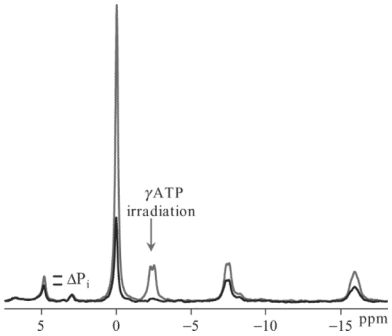

Figure 21.3.

In vivo muscle ^{31}P spectra acquired from the soleus-gastrocnemius muscle complex during a saturation-transfer experiment. Spectra are acquired with (black spectrum) and without (gray spectrum) frequency-selective irradiation of the γ-ATP peak. The rate constant of exchange $\left(k_{\mathrm{f}}^{'}\right)$ is equivalent to the decrease in the P_i peak upon γATP saturation $\left(\Delta P_i \Rightarrow 1 - M_{Pi}^{'}/M_0^{Pi}\right)$ divided by the T_1 relaxation time $\left(T_1^{'}\right)$. $V_{ATP}=k_{\mathrm{f}}^{'}[P_i]$.

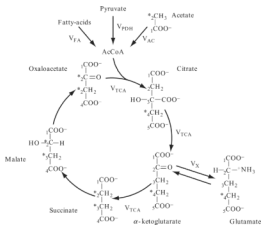

Figure 21.4.

Oxidation via the TCA cycle: substrate derived from carbohydrate and lipid enters the cycle via the common intermediate acetyl CoA. Infused plasma [2-^{13}C]-acetate is converted to acetyl CoA, and the ^{13}C label (denoted by *) becomes incorporated into the muscle TCA-cycle intermediate and glutamate pools forming [4-^{13}C] glutamate on the first turn of the TCA cycle. The ^{13}C label becomes scrambled between the C_2 and C_3 positions due to the symmetry of the succinate molecule; a second turn of the cycle forms [2-^{13}C] and [3-^{13}C]-glutamate. Reaction rates incorporated into the metabolic model to calculate the TCA cycle flux (V_{TCA}) are shownand described in the text. Adapted and reprinted from Befroy *et al*. (2008a);

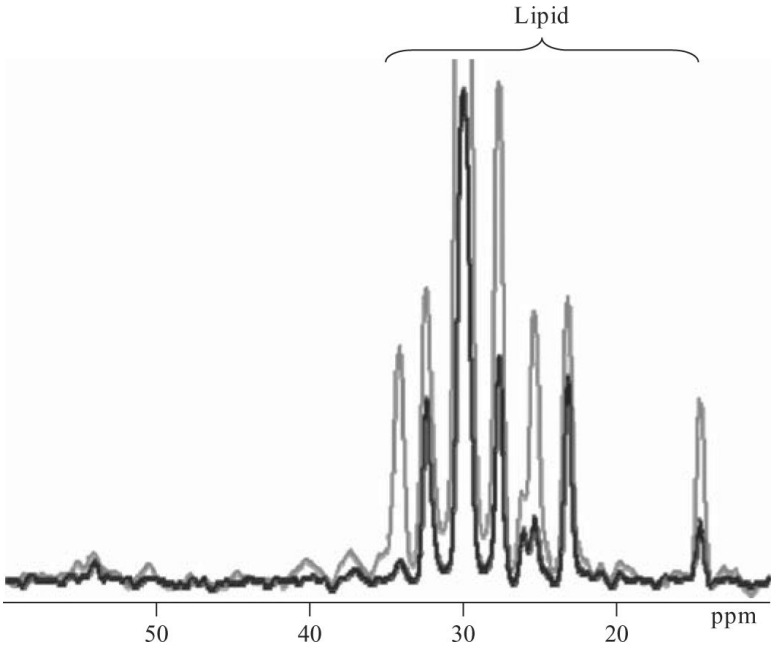

Figure 21.5.
Natural abundance ^{13}C spectra acquired from the soleus-gastrocnemius muscle complex demonstrating the use of lipid suppression techniques to minimize the contribution of subcutaneous fat and IMCL resonances to the spectrum.

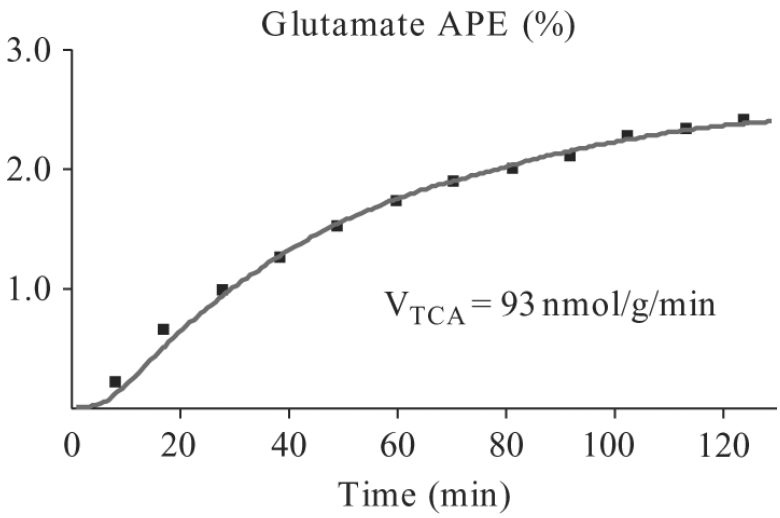

Figure 21.6.

Time course of muscle [4-^{13}C]-glutamate enrichment measured by ^{13}C MRS in a typical healthy individual during a [2-^{13}C]-acetate infusion. The fit of the data using the CWave metabolic model of the TCA cycle is superimposed along with the calculatedTCA cycle flux (V_{TCA}).

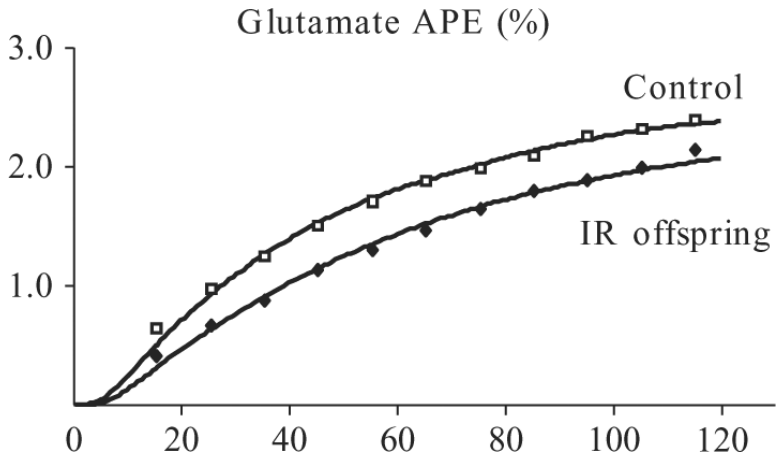

Figure 21.7.
Muscle [4-^{13}C]-glutamate enrichment (averaged data) measured by ^{13}C MRS in a group of healthy, insulin-sensitive control subjects and insulin-resistant (IR) offspring of type 2 diabetic patients. CWave fits of the data are superimposed demonstrating the difference in the rates of enrichment and the resultant TCA cycle flux between the groups. Adapted and reprinted from Befroy *et al*. (2007); © American Diabetes Association (ADA).